A New Torque and Flux Controller for Direct Torque Control of Induction Machines

Nik Rumzi Nik Idris, *Senior Member, IEEE*, Chuen Ling Toh, and Malik E. Elbuluk, *Senior Member, IEEE*

***Abstract*—This paper presents the implementation of a high-performance direct torque control (DTC) of induction machines drive. DTC has two major problems, namely, high torque ripple and variable switching frequency. In order to solve these problems, this paper proposed a pair of torque and flux controllers to replace the hysteresis-based controllers. The design of these controllers is fully discussed and a set of numerical values of the parameters for the proposed controllers is given. The simulation of the proposed controllers applied to the DTC drive is presented. The simulation results are then verified by experimental results. The hardware implementation is mainly constructed by using DSP TMS320C31 and Altera field-programmable gate array devices. The results prove that a significant torque and stator flux ripples reduction is achieved. Likewise, the switching frequency is fixed at 10.4 kHz and a more sinusoidal phase current is obtained.**

***Index Terms*—Constant switching frequency, direct torque control (DTC), DSP control implementation, field-programmable gate arrays (FPGAs), flux controller, induction machines, torque controller, torque ripple.**

I. Introduction

NOT UNTIL the mid 1980s, when direct torque control (DTC) was first introduced, was field-oriented control (FOC) of induction machines considered the only scheme capable of delivering high-performance torque control in ac machines [1]. The first DTC drive was marketed by ABB in 1996 and since then has gained popularity in applications, which previously utilized FOC drives. In DTC, the torque and flux are directly controlled using optimum voltage vectors; whereas, the FOC, which uses q- and d-axis components of the stator current to control the torque and flux, respectively, require current regulated pulsewidth modulation or space-vector modulation (SVM) for implementation. Unlike the FOC drives, where frame transformation is a must, no frame transformation is required in DTC, and in its basic configuration, only the stator resistance is required to estimate the stator flux and torque. It is also shown that DTC of induction machine gives faster torque response compared to the FOC of induction machines. The basic configuration of the conventional DTC drive consists of a pair of hysteresis comparators, torque and flux estimators, a voltage vector selector, and a voltage source inverter. Although gaining popularity, DTC has some drawbacks, which need to be rectified. Variable switching frequency and high torque and flux ripples are the major problems.

The root of variable switching frequency in DTC is the use of torque and flux hysteresis controllers, as originally proposed in [1]. Hysteresis controllers not only produce a variable switching frequency but also produce large torque and flux ripples. Therefore, various methods have been proposed to overcome these problems including the use of variable hysteresis bands [2], predictive control schemes [3], SVM [4], and intelligent control techniques [5]. The use of these techniques, however, has somehow increased the complexity of the control technique in DTC and diminished the main feature of DTC, which is simple control structure.

A torque controller, which produces constant torque switching frequency with low ripple, has been presented in [6]–[8]. The method replaces the conventional hysteresis torque comparator with a fixed switching frequency controller. Subsequently, an almost fixed switching frequency is obtained by comparing the triangular waveforms with the compensated torque error signal. There are two major limitations associated with the method presented in [6] and [7]. First, since the triangular waveform is generated by the digital signal processor, which is also responsible for performing other tasks, the frequency of the triangular wave, hence the switching frequency, is limited by the sampling period of the processor. Second, the switching frequency still varies with operating conditions. This is mostly due to the fact that the flux controller still uses the hysteresis-based comparator. In [8], we have removed the first limitation by introducing the field-programmable gate array (FPGA) to perform some of the important tasks, hence reducing the burden of the processor. The tasks include the generation of the high-frequency triangular waveform, performing the comparisons, as well as the implementation of the lookup table. By doing so, we have managed to increase the torque switching frequency from 2.7 kHz (in [6] and [7]) to about 10 kHz (in [8]).

This paper expands on the work presented in [6]–[8]. Instead of just the hystersis-based torque controller as in [6]–[8], here, we also replace the flux hysteresis-based controller with a constant frequency controller. The consequences of introducing this new flux controller are twofold. First, it would remove

Paper MSDAD-06-07 presented at the 2005 Industry Applications Society Annual Meeting, Hong Kong, October 2–6, and approved for publication in the IEEE TRANSACTIONS ON INDUSTRY APPLICATIONS by the Industrial Automation and Control Committee of the IEEE Industry Applications Society. Manuscript submitted for review October 15, 2005 and released for publication July 21, 2006.

N. R. N. Idris is with the Electrical Energy Conversion Department, Universiti Teknologi Malaysia, 81310 UTM, Skudai, Malaysia (e-mail: nikrumzi@ieee.org).

C. L. Toh was with the Electrical Energy Conversion Department, Universiti Teknologi Malaysia, 81310 UTM, Skudai, Malaysia. She is now with Intel Microelectronics (M) Sdn. Bhd. (Company No. 302251-K), Penang, Design Center (PG12), Halaman Kampung Jawa, 11900 Penang, Malaysia (e-mail: chuen.ling.toh@intel.com).

M. E. Elbuluk is with the Department of Electrical and Computer Engineering, University of Akron, Akron, OH 44325-3904 USA (e-mail: melbuluk@uakron.edu).

Color versions of Figs. 13–15 are available at http://ieeexplore.ieee.org.

Digital Object Identifier 10.1109/TIA.2006.882685

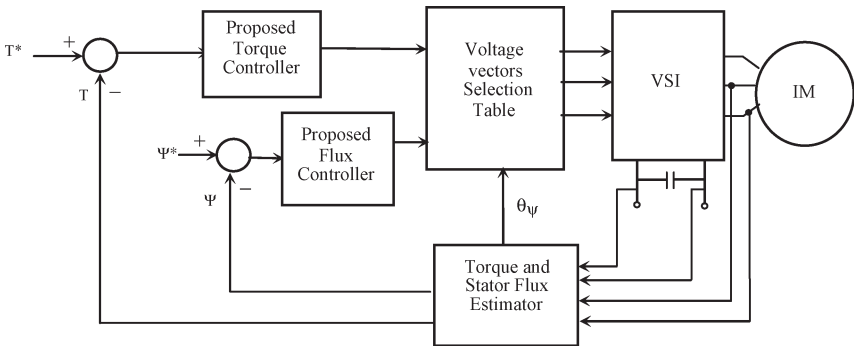

Fig. 1. DTC drive with proposed torque and flux controllers.

the influence the flux hysteresis-based comparator can have on the switching frequency. Second, the phase current distortion significantly improves as a result of the low flux ripple. In this paper, the development of the averaged, linearized torque and flux loops, which are used to systematically select the parameters of the controllers, is fully discussed. A set of numerical values of the parameters for the proposed controllers is also given. Due to the principle of the controllers, which is based on waveform comparisons, the implementation is relatively easy. The FPGA device was used to perform the waveform comparisons and the DSP was used to estimate the torque and stator flux.

The rest of this paper is organized as follows. Section II presents the principle and modeling of the proposed controllers. Section III discusses the design and implementation of the controllers with some simulation and experimental results. Finally, Section IV draws conclusions.

II. Proposed Torque and Flux Controllers

The proposed DTC consists of two controllers, namely a torque controller and a flux controller, as shown in Fig. 1. The operations of the new torque and flux controllers are similar to the torque controller proposed in [6] and [7] but with a higher triangular wave frequency. This is made possible since the triangular waves and the comparisons are performed using the FPGA and no longer the tasks of the DSP. The maximum switching capability of the devices can be fully utilized since the switching frequency is independent of the operating conditions and equals the frequency of the triangular waves. These controllers are easily implemented utilizing digital circuits since it just involves comparison of waveform rather than complicated calculation of duty cycles or voltage vectors.

A. Torque Controller

The proposed torque controller consists of two triangular waveform generators, two comparators, and a proportional–integral (PI) controller as shown in Fig. 2. The two triangular waveforms ($C_{\rm upper}$ and $C_{\rm lower}$) are 180° out of phase with each other. The absolute values of the dc offsets for the triangular waveforms are set to half of their peak–peak values. The possible instantaneous output of the proposed torque controller $qt(t)$ is similar to the well-known three-level hysteresis comparator used in DTC drives, i.e., it can be one of the three states: -1, 0, or 1. This output follows the conditions given in (1). Similar to the hysteresis-based DTC, the output is used to determine

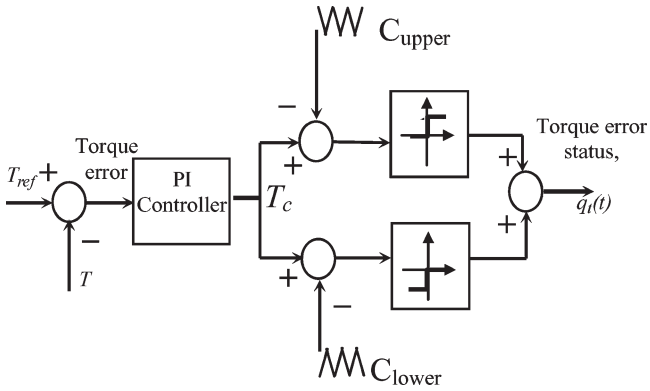

Fig. 2. Proposed torque controller.

TABLE I
Voltage Vectors Lookup Table

CCW (CC)		Sec I	Sec II	Sec III	Sec IV	Sec V	Sec VI
Inc Flux	Inc T	100 (001)	110 (101)	010 (100)	011 (110)	001 (010)	101 (011)
	Dec T	000 (000)	111 (111)	000 (000)	111 (111)	000 (000)	111 (111)
Dec Flux	Inc T	110 (011)	010 (001)	011 (101)	001 (100)	101 (101)	100 (010)
	Dec T	111 (111)	000 (000)	111 (111)	000 (000)	111 (111)	000 (000)

CW = clockwide rotation
CCW = counter-clockwise rotation

the voltage vectors that will increase or reduce the torque. A similar lookup table as employed in [1] is used to determine the suitable voltage vectors, which is tabulated in Table I. The table is constructed based on sectors of the stator flux plane shown in Fig. 3. CW refers to the clockwise rotation, while CCW is for counterclockwise

$$q_t(t) = \begin{cases} 1, & \text{for } T_{\rm c} \geq C_{\rm upper} \\ 0, & \text{for } C_{\rm lower} < T_{\rm c} < C_{\rm upper} \\ -1, & \text{for } T_{\rm c} \leq C_{\rm lower} \end{cases} . \quad (1)$$

The average torque error status is defined as continuous duty ratio, denoted by $d_t(t)$, taken over an interval $T_{\rm T,tri}$, which is the period of the triangular wave.

$$d_t(t) = \frac{1}{T_{\rm T,tri}} \int_{t}^{t+T_{\rm T,tri}} q_t(t)dt. \quad (2)$$

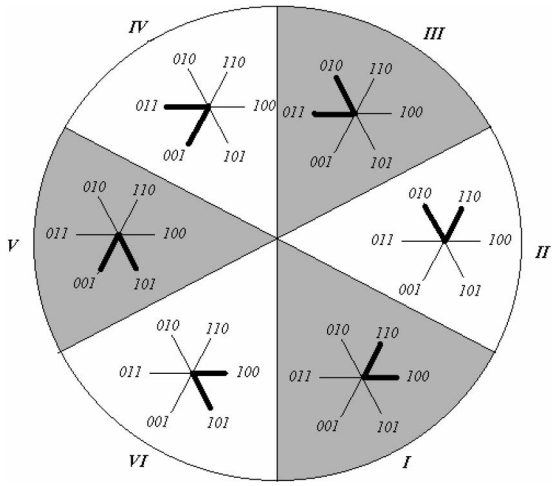

Fig. 3. Sectors for stator flux plane. Thick vectors in each sector are vectors used to increase or decrease flux in counterclockwise direction.

In order to properly design the PI controller, a small signal model of the torque loop has to be developed. The space vector equations of induction machine expressed in general reference frame rotating at $\omega_{\rm g}$ are given by

$$\overline{v}_{\rm s}^{\rm g} = R_{\rm s}\bar{i}_{\rm s}^{\rm g} + \frac{d\overline{\psi}_{\rm s}^{\rm g}}{dt} + j\omega_{\rm g}\overline{\psi}_{\rm s}^{\rm g} \tag{3}$$

$$O = R_{\rm r}\bar{i}_{\rm r}^{\rm g} + \frac{d\overline{\psi}_{\rm r}^{\rm g}}{dt} + j(\omega_{\rm g} - \omega_{\rm r})\overline{\psi}_{\rm r}^{\rm g} \tag{4}$$

where $\bar{v}_{\rm r}^{\rm g}$ and $\bar{i}_{\rm r}^{\rm g}$ are the voltage and current space vectors, while $R_{\rm s}$ and $R_{\rm r}$ are the stator and rotor resistances, respectively. $\bar{\psi}_{\rm s}^{\rm g}$ and $\bar{\psi}_{\rm r}^{\rm g}$ are the stator and rotor flux linkages, respectively, and are given by

$$\overline{\psi}_{\rm s}^{\rm g} = L_{\rm s}\bar{i}_{\rm s}^{\rm g} + L_{\rm m}\bar{i}_{\rm r}^{\rm g} \tag{5}$$

$$\overline{\psi}_{\rm r}^{\rm g} = L_{\rm r}\bar{i}_{\rm r}^{\rm g} + L_{\rm m}\bar{i}_{\rm s}^{\rm g} \tag{6}$$

where $L_{\rm s}$ and $L_{\rm r}$ are the stator and rotor self-inductance, respectively. The superscript "g" in (3)–(6) denotes that the quantity is referred to the general reference frame. The torque $T_{\rm e}$ and mechanical dynamics of the machines are modeled by

$$T_{\rm e} = \frac{3}{2}\frac{p}{2}\overline{\psi}_{\rm s}^{\rm g} \times \bar{i}_{\rm s}^{\rm g} \tag{7}$$

$$J\frac{d\omega_{\rm m}}{dt} = J\frac{2}{p}\frac{d\omega_{\rm r}}{dt} = T_{\rm e} - T_{\rm load} \tag{8}$$

where J and p are the moment of inertia and the number of poles, respectively.

It has been shown in [6] that using the space vector equations of the induction machine given in (3)–(6), the positive and negative torque slopes expressed in stator flux reference frame can be written as

$$\frac{dT_{\rm e}^{+}}{dt} = -\frac{T_{\rm e}}{\sigma\tau_{\rm sr}} + \frac{3p}{4}\frac{L_{\rm m}}{\sigma L_{\rm s}L_{\rm r}}\left[v_{\rm s}^{\psi_{\rm s}}\psi_{\rm s} - (\omega_{\rm r} - \omega_{\psi_{\rm s}})\cdot\left(\psi_{\rm s}\psi_{\rm r}^{\psi_{\rm s}}\right)\right] \tag{9}$$

$$\frac{dT_{\rm e}^{-}}{dt} = -\frac{T_{\rm e}}{\sigma\tau_{\rm sr}} - \frac{3p}{4}\frac{L_{\rm m}}{\sigma L_{\rm s}L_{\rm r}}\left[(\omega_{\rm r} - \omega_{\psi_{\rm s}})\cdot\left(\psi_{\rm s}\psi_{\rm r}^{\psi_{\rm s}}\right)\right] \tag{10}$$

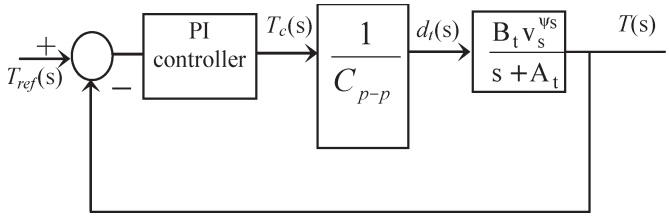

Fig. 4. Small signal torque loop.

where $1/\tau_{\rm sr} = ((1/\tau_{\rm s}) + (1/\tau_{\rm r}))$, and $\tau_{\rm s}$, $\tau_{\rm r}$ represent the stator and rotor time constants, respectively. σ is the total leakage factor. The superscript $\omega_{\psi_{\rm s}}$ in (9) and (10) indicates that quantities are referred to the stator flux reference frame. If $f_{\rm T,tri}$ is the frequency of the triangular wave, and assuming over one cycle of $f_{\rm T,tri}$ an active and a zero voltage vectors are selected, then over one cycle of the synchronous frequency $\omega_{\rm e}$, the number of active voltage vector selected is given by $2\pi f_{\rm T,tri}/\omega_{\rm e}$. Since the stator flux only moves when an active voltage is applied, the incremental change in stator flux angle $\Delta\theta$ is given by $2\pi\omega_{\rm e}/2\pi f_{\rm T,tri}$. The duration in which each active voltage vector applied Δt is $d_t/f_{\rm T,tri}$. Therefore, the ratio between the small change in stator flux angle $(\Delta\theta)$ and the duration of each applied active voltage vectors (Δt) is given by

$$\frac{\Delta\theta}{\Delta t} = \frac{\left(\frac{2\pi\omega_{\rm e}}{2\pi f_{\rm T,tri}}\right)}{\frac{d_t}{f_{\rm T,tri}}} = \frac{\omega_{\rm e}}{d_t}. \tag{11}$$

Assuming that Δt is small enough such that the change in stator flux is linear, (11) approximates the instantaneous stator flux frequency $\omega_{\psi_{\rm s}}$. Therefore, the instantaneous stator flux frequency can be expressed in terms of synchronous frequency and average duty ratio d_t. Since $\omega_{\rm e} = \omega_{\rm slip} + \omega_{\rm r}$, we can write

$$\omega_{\psi_{\rm s}} = \frac{\omega_{\rm slip} + \omega_{\rm r}}{d_t}. \tag{12}$$

Substituting (12) into (9) and (10) and averaging these equations [6] gives

$$\frac{dT_{\rm e}}{dt} = -A_t T_{\rm e} + B_t v_{\rm s}^{\psi_{\rm s}} d_t + K_t(\omega_{\rm slip}) \tag{13}$$

where $A_t = 1/\sigma\tau_{\rm sr}$, $B_t = (3p/4)(L_{\rm m}/\sigma L_{\rm s}L_{\rm r})\psi_{\rm s}$, and $K_t = (3p/4)(L_m/\sigma L_{\rm s}L_{\rm r})(\psi_{\rm s}\psi_{\rm r}^{\psi_{\rm s}})$. In (13), it is assumed that the magnitudes of the stator and rotor fluxes are held constant. Equation (13) can now be transformed to frequency domain and linearized by introducing a small perturbation in $T_{\rm e}$, d_t, and $\omega_{\rm slip}$. Taking Laplace of the ac components and rearranging terms, the torque $T_{\rm e}({\rm s})$ can be written as

$$\tilde{T}_{\rm e}(s) = \frac{B_t v_{\rm s}^{\psi_{\rm s}}\tilde{d}_t(s) + K_t\tilde{\omega}_{\rm slip}(s)}{s + A_t}. \tag{14}$$

The term contributed by the slip frequency is relatively small and hence for simplicity will be neglected. Hence, the small signal torque loop is shown in Fig. 4. C_{p-p} in Fig. 4 is the peak–peak triangular waveform. Ideally, we want the torque

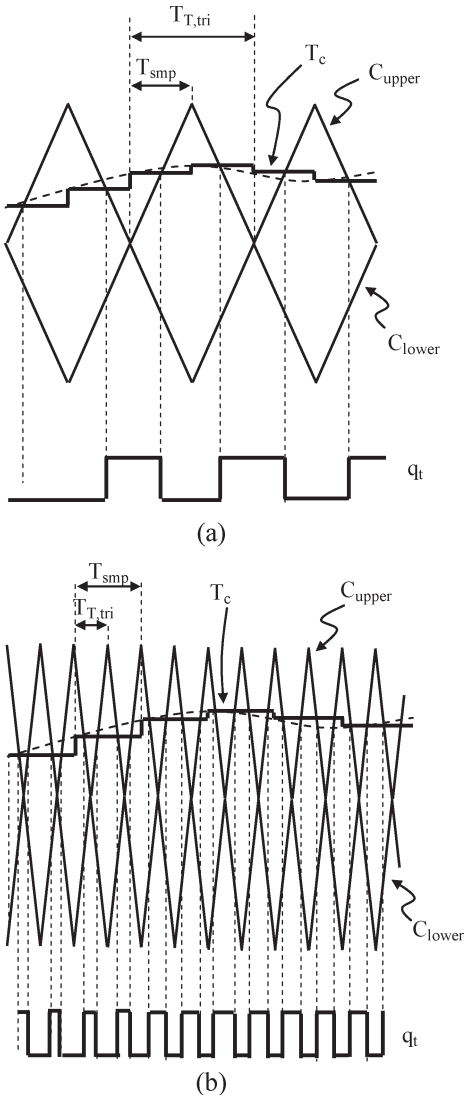

Fig. 5. Timing diagram of $C_{\rm upper}$, $C_{\rm lower}$, $T_{\rm c}$, and q: (a) for $T_{\rm smp} < T_{\rm T,tri}$ and (b) for $T_{\rm smp} > T_{\rm T,tri}$.

loop bandwidth to be as large as possible to obtain a fast torque response. However, the bandwidth is constrained by either the period of the triangular wave $T_{\rm T,tri}$ or the sampling period of the processor $T_{\rm smp}$. Fig. 5(a) shows the timing diagram of $C_{\rm upper}$, $C_{\rm lower}$, $T_{\rm c}$, and q_t when $T_{\rm T,tri} = 2T_{\rm smp}$. Under this condition, we must ensure that the torque loop bandwidth is much lower than the frequency of the triangular wave. On the other hand, Fig. 5(b) is the timing diagram when $2T_{\rm T,tri} = T_{\rm smp}$. The torque control works if the torque loop bandwidth is lower than the sampling frequency. Notice that the switching of the output signal q_t is determined by the frequency of the triangular wave. This simply means that we can ideally increase the inverter switching frequency higher than the sampling frequency provided that the bandwidth is set to be much lower than the sampling frequency. Since the triangular waveform is generated using the FPGA device, its frequency can be set a few times higher than the processor sampling frequency. It is, however, necessary to synchronize the sampling and the triangular waveforms.

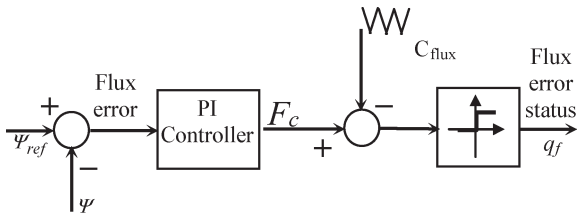

Fig. 6. Proposed flux controller.

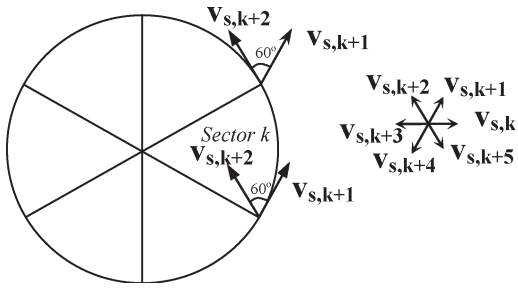

Fig. 7. Circular flux locus.

B. Flux Controller

The proposed flux controller is shown in Fig. 6, which in principle works similarly to that of the torque controller. As in the hysteresis-based controller, there are only two levels of output generated from the controller, i.e., "1" to increase the flux and "0" to reduce the flux. This implies that only a single triangular waveform, denoted by $C_{\rm flux}$, is required. For a given synchronous frequency, the switching frequency of the flux controller only depends on the frequency of the triangular wave. The output of the controller is given by

$$q_{\rm f}(t) = \begin{cases} 1, & \text{for } F_{\rm c} \geq C_{\rm flux} \\ 0, & \text{for } F_{\rm c} < C_{\rm flux} \end{cases}. \tag{15}$$

For a triangular period of $T_{\rm F,tri}$, its average value is given by

$$d_{\rm f}(t) = \frac{1}{T_{\rm F,tri}} \int_{t}^{t+T_{\rm F,tri}} q(t)dt. \tag{16}$$

For the sake of simplicity, we will assume that the stator resistance drop is negligible; hence, using (3), the slope of the flux in stationary reference frame can be approximated by (17), which simply indicates that it is totally dependent on the selected voltage vectors

$$\text{slope} \equiv \frac{d\overline{\Psi}}{dt} = \overline{v}_{\rm s}. \tag{17}$$

The derivative of the stator flux vector at t is the tangent vector of the stator flux to the curve traced by $\bar{\psi}_{\rm s}$ at t. Therefore, the slope depends on the stator flux position and it can be seen from Fig. 7 that at every entrance to a sector, the magnitude of the positive and negative slopes are zero and maximum, respectively.

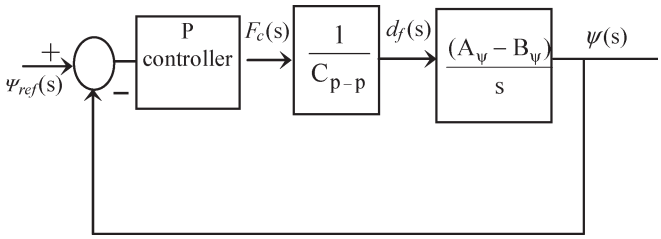

Fig. 8. Small signal flux loop.

If θ is the angle of the stator flux relative to the sector it enters, the positive and negative slopes can be written as

$$\left.\begin{aligned} \text{slope}^+ &\equiv \frac{2}{3}V_{\rm dc}\sin\theta \\ \text{slope}^- &\equiv -\frac{2}{3}V_{\rm dc}\sin\left(\theta+\frac{2}{3}\pi\right) \end{aligned}\right\}. \tag{18}$$

Equation (18) indicates that relation between the rate of change stator flux magnitude and the stator flux position θ is nonlinear because of the sinusoidal functions. The slope varies nonlinearly with flux position and repeats for every sector. In order to simplify the analysis, it will be assumed that the slope is constant during which the flux error status is one or zero. Then, it is possible to obtain the average positive and negative slopes by averaging them over a sector. This is easily done since we know the number of positive or negative slopes within a sector is given by $N_{\rm f} = (2\pi f_{\rm F,tri})/6\omega_{\rm e}$. The average positive and negative slope can be calculated as

$$\frac{d\Psi^+}{dt} = \frac{1}{N_{\rm f}}\sum_{n=0}^{N_{\rm f}}\frac{2}{3}V_{\rm dc}\sin\left(\frac{\frac{\pi}{3}}{N_{\rm f}}\right)n = A_\psi \tag{19}$$

$$\frac{d\Psi^-}{dt} = -\frac{1}{N_{\rm f}}\sum_{n=0}^{N_{\rm f}}\frac{2}{3}V_{\rm dc}\sin\left(\left(\frac{\frac{\pi}{3}}{N_{\rm f}}\right)n+\frac{2}{3}\pi\right) = B_\psi \tag{20}$$

which gives an average slope of

$$\frac{d\Psi}{dt} = (A_\psi - B_\psi)d_{\rm f} + B_\psi. \tag{21}$$

Introducing a small perturbation in ψ and $d_{\rm f}$, the transfer function between ψ and d can be obtained as

$$\frac{\tilde{\Psi}}{\tilde{d}_{\rm f}} = \frac{(A_\psi - B_\psi)}{s}. \tag{22}$$

Finally, the small signal flux loop is shown as in Fig. 8. C_{p-p} is the peak to peak of the triangular wave used in the flux controller. It is clear from the small signal model that only a proportional-type controller is required to obtain zero steady-state error in flux response. Similar to torque control, the bandwidth is limited by the frequency of the triangular wave or the sampling frequency, depending on which one is lower. Provided that the sampling is synchronized with the triangular waveform, the switching frequency can be made higher than the bandwidth of the flux loop.

TABLE II
PARAMETERS OF INDUCTION MACHINE AND SETTINGS

Stator resistance	10.9 Ω
Rotor resistance	9.5 Ω
Stator self inductance	0.859 H
Rotor self inductance	0.859 H
Mutual inductance	0.828 H
Rated speed	2880 rpm
Pole pair	2
DC link voltage	120 V
Rated flux	0.495 Wb

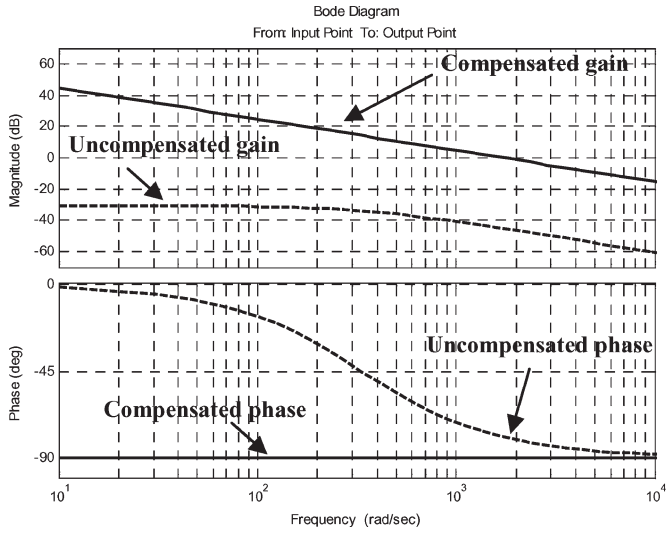

Fig. 9. Bode plot of torque open-loop gain before and after compensation.

III. SIMULATION, IMPLEMENTATION RESULTS, AND DISCUSSION

Three different sets of simulations and experiments were carried out as follows:

1) hysteresis torque and flux controllers;
2) proposed torque controller and hysteresis flux;
3) proposed torque and flux controllers.

The simulations of the DTC drive were carried out using Matlab/Simulink simulation package. The parameters of the induction machine used in the simulation and experiment are listed in Table II.

In this paper, the sampling period of the DSP $T_{\rm smp}$ is 48 μs ($f_{\rm smp} = 20\,833$ kHz), while the period of the triangular wave $T_{\rm T,tri}$ is at about 96 μs ($f_{\rm tri} = 10.4$ kHz). Based on the discussion from the previous section, since $T_{\rm smp} < T_{\rm T,tri}$, the bandwidth is primarily limited by the frequency of the triangular wave. The Bode plot of the open-loop gain for the torque loop, without the PI controller, is shown by the dashed line in Fig. 9. Clearly, without compensation, the response would be unacceptable. In this paper, the zero of the PI controller is selected to approximately cancel the pole of the open-loop gain. Subsequently, the gain is adjusted to give the desired bandwidth, which is much lower than 10 kHz. Using the design procedure described in Section II, proportional and integral constants for the PI torque controller were calculated as $K_{\rm p} = 180$ and $K_{\rm i} = 60\,000$. With these values, the torque loop bandwidth is found out to be 1885 rad/s. The Bode plot of the compensated open-loop gain is shown by a solid line in Fig. 9. It should be noted

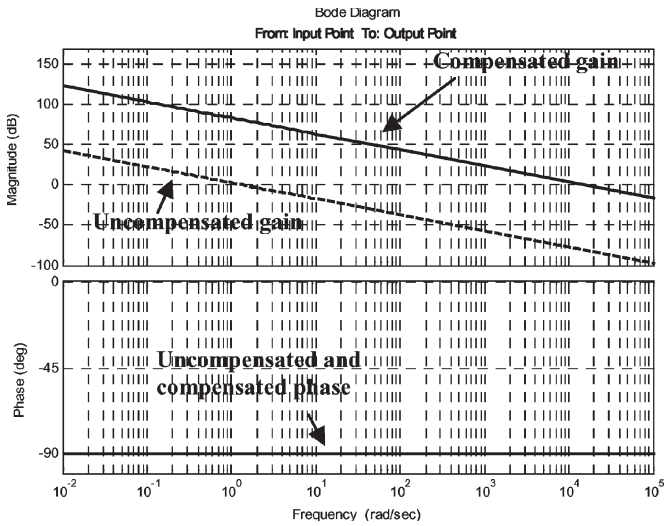

Fig. 10. Bode plot of flux open-loop gain before and after compensation.

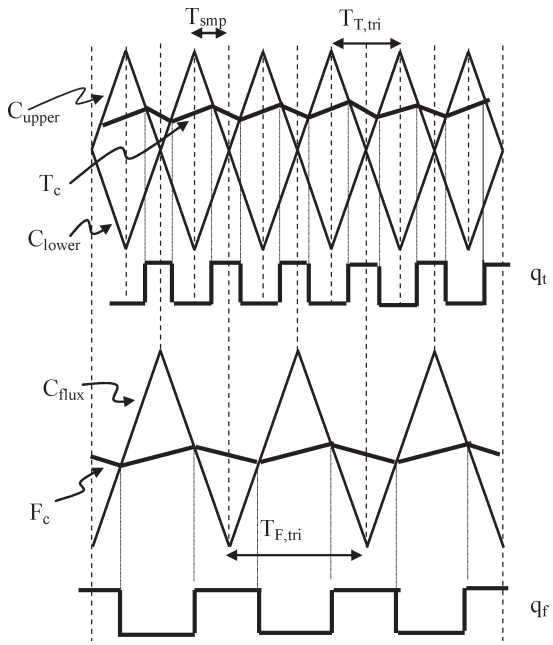

Fig. 11. Ideal timing diagram of proposed torque and flux controllers.

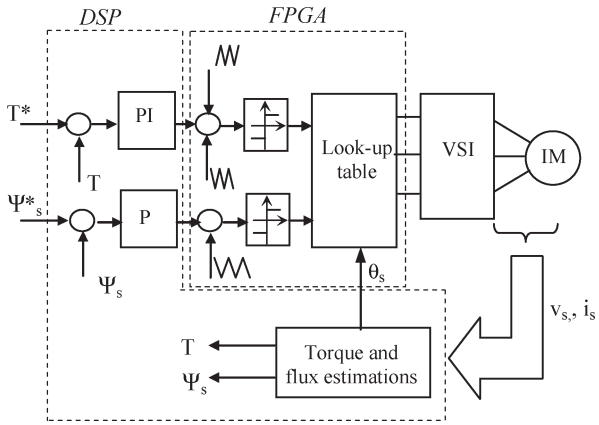

Fig. 12. Implementation of proposed controllers using DSP and FPGA.

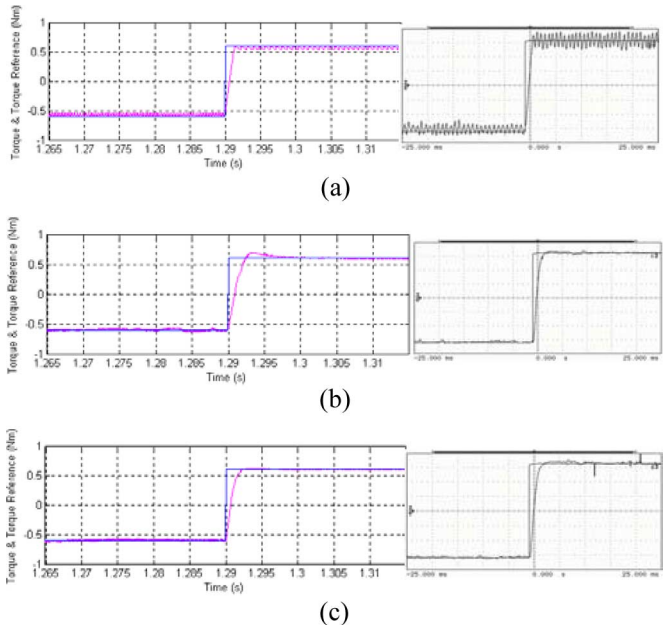

Fig. 13. Simulation and experimental step torque response. Experimental results scale of 0, 2 N · m/div. (a) Hysteresis torque and flux controllers. (b) Proposed torque and hysteresis flux controllers. (c) Proposed torque and flux controllers.

that it is possible to increase the inverter switching frequency higher than the processor sampling frequency by increasing the frequency of the triangular wave. Under this condition, the controller should be designed such that the bandwidth is primarily constrained by the processor sampling frequency rather than the frequency of the triangular wave.

The Bode plot of the open-loop gain for the flux loop without the P controller is shown by the dashed line in Fig. 10. Since the loop includes a pole at the origin, ideally, only a proportional controller is required to produce zero steady-state flux error. The bandwidth can be adjusted by simply varying the gain of the flux proportional controller and it is primarily constrained by the frequency of the flux triangular wave. The bandwidth should be lower than the frequency of the flux triangular wave, which is, for this particular implementation, at 5 kHz. It should be noted that in developing the flux loop model, it is assumed that selecting zero voltage vectors will ideally halt the flux; whereas, in practice, the flux will be slightly weakened due to the presence of the stator resistance especially at light load and low speed. This will effectively reduce the open-loop gain and should be considered when selecting the flux bandwidth. Based on simulations and experiments, it was found out that the value of $K_{\rm pf} = 11\,000$ produced a good flux response. This corresponds to a flux bandwidth of 15 268 rad/s, as can be seen by the solid line of Fig. 10.

A. Implementation of Proposed Controllers

The major parts of the controllers were composed of a DSP and an FPGA device. With this combination, it is possible to generate the triangular waveforms at frequencies close to or higher than the sampling frequency of the DSP. Therefore,

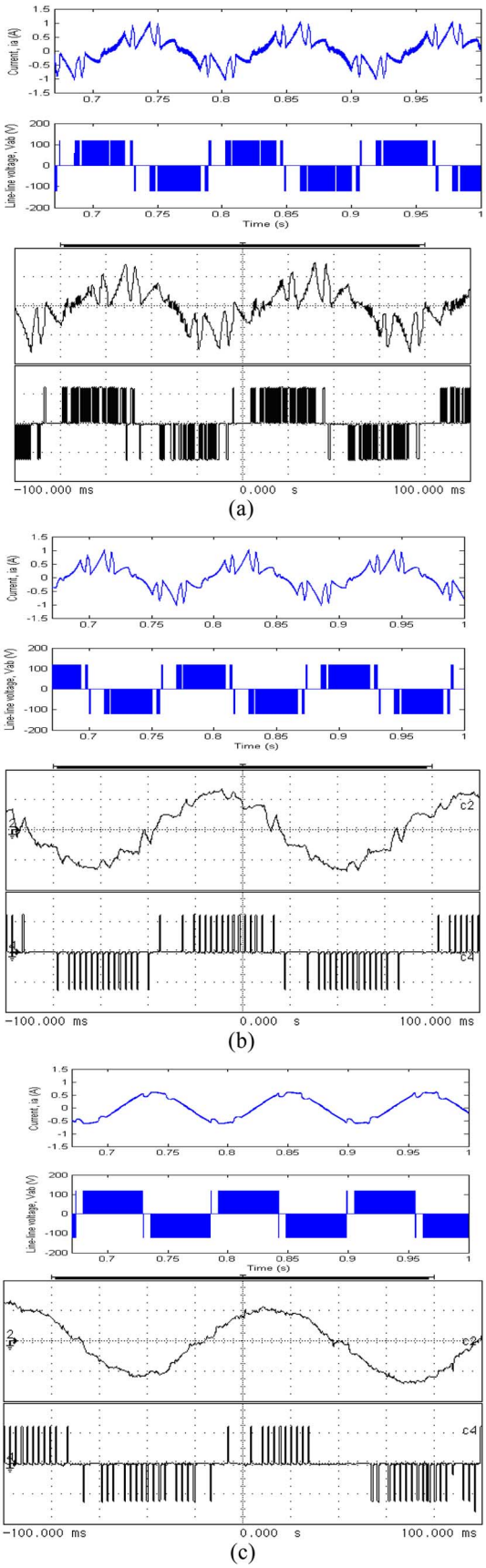

Fig. 14. Simulation and experimental (0.5714 A/div, 100 V/div) results of steady-state phase current and line–line voltage. (a) Hysteresis-based torque and flux controllers. (b) Proposed torque and hysteresis-based flux controllers. (c) Proposed torque and flux controllers.

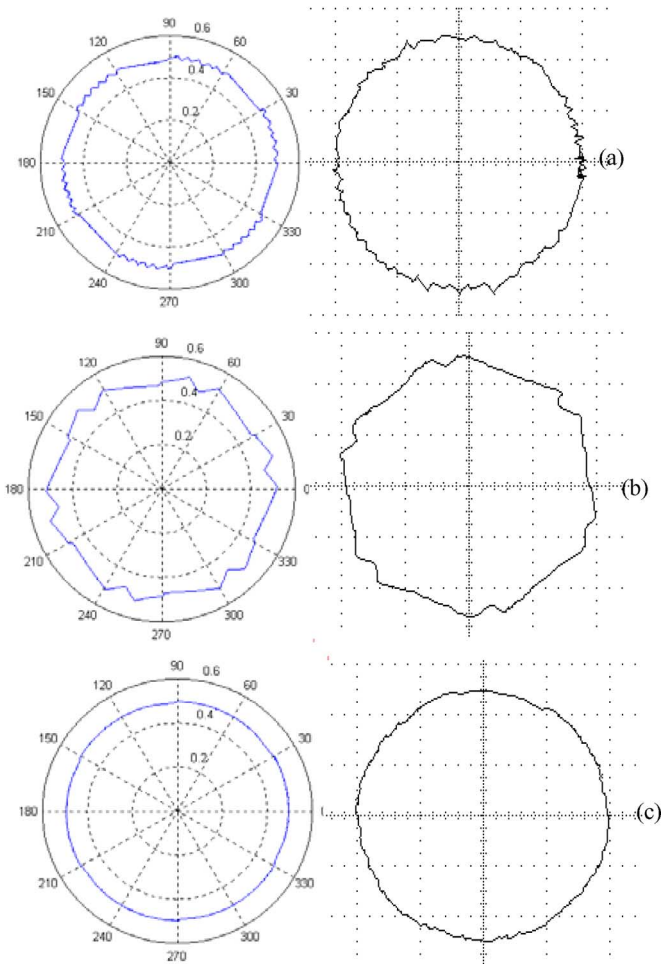

Fig. 15. Simulation and experimental stator flux locus (0.2 Wb/div) for (a) hysteresis-based torque and flux controllers, (b) proposed torque and hysteresis-based flux controllers, and (c) proposed torque and flux controllers.

as discussed in the previous section, it is possible to increase the switching frequency of the inverter much higher than the sampling period.

The DSP board (DS1102) from dSPACE, based on TMS320C31 operating at 60 MHz, was used in this paper. It was mainly used to estimate the torque and stator flux using the stator current and voltage, which were sampled at 20.8 kHz ($T_{\rm smp} = 48\ \mu$s). Other than this, the DSP was also responsible for: 1) implementing the PI and P controllers for the torque and flux loops, respectively, and 2) determining the sector of the stator flux. These values were then passed to the Altera EPF10K20 FPGA device contained on an Altera UP1 Educational Board. Very high-speed integrated circuits hardware description language was utilized in digital logic designs of the FPGA. The design was then compiled and simulated using MAX + PLUS II and finally downloaded to the EPF10K20 device. Since the triangular waveforms of the torque and flux controllers were generated using FPGA, their frequencies were not constrained by the clock speed of the DSP. In this paper, the frequencies of the triangular waves for the torque and flux controllers are set to 10.4 and 5.2 kHz, respectively, and they are synchronized with the sampling frequency of the DSP of 20.8 kHz—this is illustrated in Fig. 11.

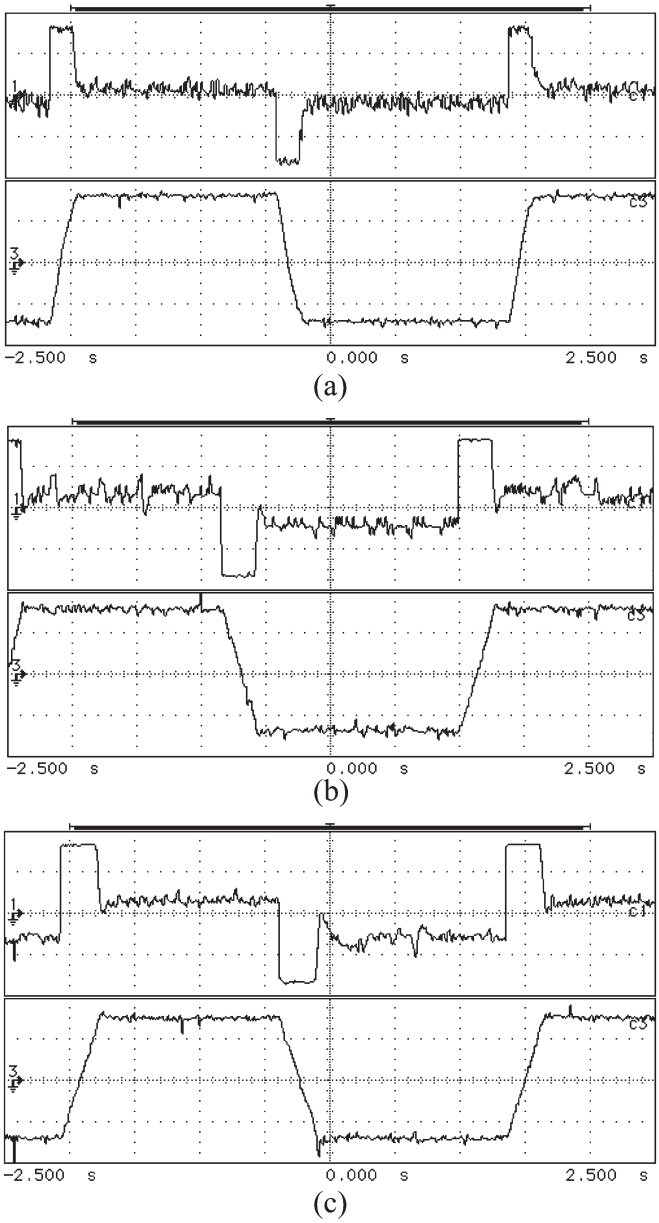

Fig. 16. Experimental results. Torque (1 N · m/div) and speed (9.33 rad/s/div) response with square wave speed reference. (a) Hysteresis torque and flux controllers. (b) Proposed torque and hysteresis-based flux controllers. (c) Proposed torque and flux controllers.

The torque and flux errors, which were obtained from the DSP, were compared with the triangular waveforms within the FPGA. From the comparison results and the location of the stator flux, suitable voltage vectors were selected based on the lookup table implemented within the FPGA and are given in Table I. The various tasks of the DSP and the FPGA were summarized in Fig. 12.

B. Results and Discussion

Fig. 13 shows the simulation and experimental results of a torque response for a step reference step from -0.6 to 0.6 N · m. Experimental results for the torque and flux hysteresis controllers show a significant ripple due to the sampling delay in the DSP. This cannot be seen in the simulation since the model

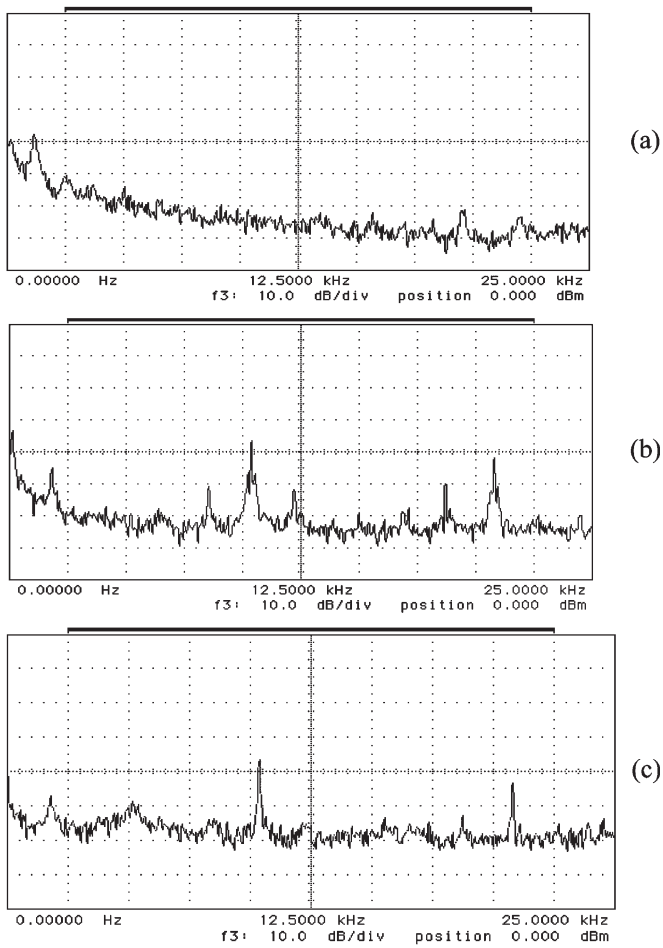

Fig. 17. Frequency spectrum of switching leg. (a) Hysteresis-based torque and flux controllers. (b) Proposed torque and hysteresis-based flux controllers. (c) Proposed torque and flux controllers.

does not include the sampling delay. All of the three sets of controllers show an excellent torque response; however, the ones with the proposed torque controller produce significant torque ripple reduction. Due to the torque bandwidth, which is constrained by the frequency of the triangular wave, the torque responses for the proposed torque controllers are slower compared to the hysteresis-based controllers. Fig. 14 shows the steady-state current and line–line voltage for the three different sets of controllers. The corresponding steady-state stator flux locus is shown in Fig. 15. Clearly, with the proposed flux controller, current distortion and hence stator flux ripple is significantly reduced.

To further examine the dynamics of the proposed controllers, a speed loop was constructed using a low-resolution incremental encoder as a speed sensor (200 ppr). A square wave speed reference was applied and the experimental results of the speed and torque responses are shown in Fig. 16. Despite of the slower torque response, the figure clearly indicates that the proposed controllers gave excellent speed dynamic performance which was as good as what can be achieved using hysteresis-based controllers, however, with an added advantage of much lower torque and flux ripples.

Finally, to look at the switching frequency of the inverter, a square wave torque reference of ± 0.6 N · m was applied

and the frequency spectrum of a switching leg was recorded as in Fig. 17. As expected, the hysteresis-based controller produced an unpredictable and dispersed switching harmonics; whereas, for the proposed controllers, the harmonic component is concentrated around the carrier frequency and its multiple. The first harmonic appeared at 10.4 kHz, which is equivalent to the torque loop triangular waveform frequency.

IV. Conclusion

This paper has presented new DTC torque and flux controllers with constant switching frequencies. Small signal modeling of the torque and flux loops has been presented. The simulation and implementation of the DTC drive with the proposed controllers were presented. From the simulation and experimental results, it is shown that despite of their simple control structure and implementation, the proposed controllers have managed to significantly reduce the torque and flux ripples. Although using the triangular wave has somehow reduced the torque and flux control bandwidths compared to the hysteresis-based controllers, this has an insignificant effect on the speed response.

References

[1] I. Takahashi and T. Noguchi, "A new quick-response and high efficiency control strategy of an induction motor," *IEEE Trans. Ind. Appl.*, vol. IA-22, no. 5, pp. 820–827, Sep.–Oct. 1986.

[2] J.-K. Kang, D.-W. Chung, and S. K. Sul, "Direct torque control of induction machine with variable amplitude control of flux and torque hysteresis bands," in *Proc. Int. Conf. Elect. Mach. Drives, IEMD*, 1999, pp. 640–642.

[3] Y. Li, J. Shao, and B. Si, "Direct torque control of induction motors for low speed drives considering discrete effect of control and dead-time timing of inverters," in *Proc. IEEE-IAS Annu. Meeting*, 1997, pp. 781–788.

[4] L. Tan and M. F. Rahman, "A new direct torque control strategy for flux and torque ripple reduction for induction motors drive by using space vector modulation," in *Proc. 32nd Annu. PESC*, 2001, vol. 3, pp. 1440–1445.

[5] S. Mir and M. E. Elbuluk, "Precision torque control in inverter-fed induction machines using fuzzy logic," in *Proc. IEEE-IAS Annu. Meeting*, 1995, pp. 396–401.

[6] N. R. N. Idris and A. H. M. Yatim, "Reduced torque ripple and constant torque switching frequency strategy for Direct Torque Control of induction machine," in *Proc. 15th IEEE-APEC*, New Orleans, LA, 2000, pp. 154–161.

[7] ——, "Direct torque control of induction machines with constant switching frequency and reduced torque ripple," *IEEE Trans. Ind. Electron.*, vol. 51, no. 4, pp. 758–767, Aug. 2004.

[8] C. L. Toh, N. R. N. Idris, and A. H. M. Yatim, "Constant and high switching frequency torque controller for DTC drives," *IEEE Power Electron. Lett.*, vol. 3, no. 2, pp. 76–80, Jun. 2005.

Nik Rumzi Nik Idris (M'97–SM'03) received the B.Eng. degree in electrical engineering from the University of Wollongong, Wollongong, Australia, the M.Sc. degree in power electronics from Bradford University, Bradford, West Yorkshire, U.K., and the Ph.D. degree from Universiti Teknologi Malaysia, Skudai, Malaysia, in 1989, 1993, and 2000, respectively.

He was a Visiting Research Associate at the University of Akron, Akron, OH, in 2002. Currently, he is an Associate Professor at the Universiti Teknologi Malaysia, and an Administrative Committee Member of the Industry Applications Societies (IAS)/Power Electronics (PELS)/Industrial Electronics (IES) Joint Chapter of IEEE Malaysia Section. His research interests include ac drive systems and DSP applications in power electronic systems.

Chuen Ling Toh received the B.Eng. degree in electrical engineering and the M.Eng. degree in power electronics, both from Universiti Teknologi Malaysia, Skudai, Malaysia, in 2002 and 2005, respectively.

She is currently with Intel Microelectronics (M) Sdn. Bhd., Halaman Kampung Jawa, Malaysia, as a Component Design Engineer involved in front-end RTL logic design. Her research interests include the field of power electronics motor drive systems and field programmable gate array applications.

Malik E. Elbuluk (S'79–M'79–SM'97) received the B.Sc. (with honors) degree from University of Khartoum, Khartoum, Sudan, and the M.S., E.E., and D.Sc. degrees from Massachusetts Institute of Technology, Cambridge, in 1976, 1980, 1981, and 1986, respectively, all in electrical engineering.

He is a Professor at the University of Akron, Akron, OH, where he has been since 1989. He was with the faculty of the Electrical and Computer Engineering Department and the Electric Power Research Center, North Carolina State University, from 1986 to 1989. He was a Summer Research Fellow at NASA Lewis Research Center, Cleveland, OH, from 1991 to 2000. His work at NASA included low-temperature electronics for space missions, modeling and simulation of the Space Station Freedom (SSF), the power by wire (PBW), the power electronic building blocks (PEBB), and the starter/generator for aircraft engines and sensorless control of electromechanical actuators (EMA) for the more electric aircraft (MEA). His teaching and research interests include the areas of power electronics, electric machines, control systems, fuzzy logic, and neural networks.

Prof. Elbuluk actively publishes and reviews papers for IEEE Conferences and Transactions, and has organized and chaired a number of sessions for the Power Electronics (PE), the Industry Application (IA) and the Industrial Electronics (IE) Societies. He was an Associate Editor for the IEEE Transactions in Power Electronics and is currently the Manufacturing Systems Development and Applications Department (MSDAD) Vice President for the IEEE Transactions on Industry Applications and also the Vice President and Technical Program Chair for the Industry Automation and Control Committee (IACC). He is a Registered Professional Engineer in the State of Ohio.